

Determination of L_{α} – H_{II} Phase Transition Temperature for 1,2-Dioleoyl-*sn*-Glycero-3-Phosphatidylethanolamine

Gilman E. S. Toombes, Adam C. Finnefrock, Mark W. Tate, and Sol M. Gruner

Department of Physics, Cornell University, Ithaca, New York 14853 USA

ABSTRACT The thermodynamic properties of fully-hydrated lipids provide important information about the stability of membranes and the energetic interactions of lipid bilayers with membrane proteins (Nagle and Scott, *Physics Today*, 2:39, 1978). The lamellar/inverse hexagonal (L_{α} – H_{II}) phase transition of 1,2-dioleoyl-*sn*-glycero-3-phosphatidylethanolamine (DOPE) water mixtures is a first-order transition and, therefore, at constant pressure, must have a thermodynamically well-defined equilibrium transition temperature. The observed transition temperature is known to be dependent upon the rate at which the temperature is changed, which accounts for the many different values in the literature. X-ray diffraction was used to study the phase transition of fully-hydrated DOPE to determine the rate-independent transition temperature, T_{LH} . Samples were heated or cooled for a range of rates, $0.212 < r < 225^{\circ}\text{C/hr}$, and the rate-dependent apparent phase transition temperatures, $T_A(r)$ were determined from the x-ray data. By use of a model-free extrapolation method, the transition temperature was found to be $T_{LH} = 3.33 \pm 0.16^{\circ}\text{C}$. The hysteresis, $|T_A(r) - T_{LH}|$, was identical for heating and cooling rates, $\pm r$, and varied as $|r|^{\beta}$ for $\beta \approx 1/4$. This unexpected power-law relationship is consistent with a previous study (Tate et al., *Biochemistry*, 31:1081–1092, 1992) but differs markedly from the exponential behavior of activation barrier kinetics. The methods used in this study are general and provide a simple way to determine the true mesomorphic phase transition temperatures of other lipid and lyotropic systems.

INTRODUCTION

Lipid energetics are important in cell signaling, protein transport, metabolic regulation, endocytotic and exocytotic events, viral fusion, and other cellular processes (Nagle and Scott, 1978). Isolated lipids form a veritable menagerie of liquid crystal structures when hydrated and their phase behavior is valuable for studying biological membranes (Tardieu et al., 1973). In recent years, a great deal of attention has been given to the lamellar/inverse-hexagonal (L_{α} – H_{II}) phase transition, because an understanding of this transition is believed to be vital to understanding membrane fusion (Kuzmin et al., 2001) and interactions with membrane proteins (Brown, 1997). The close regulation of membrane lipid composition by a wide variety of organisms provides strong support for this view (Hazel and Williams, 1990).

The first step in determining thermodynamic properties of a system is to measure the phase diagram as a function of relevant variables, such as the temperature. By symmetry considerations, the L_{α} – H_{II} transition is expected to be first order, and, therefore, at constant pressure should occur at a well-defined temperature, T_{LH} . A very commonly studied lipid that undergoes the L_{α} – H_{II} transition is 1,2-dioleoyl-*sn*-glycero-3-phosphatidylethanolamine (DOPE), which is used both because it is readily available and because T_{LH} is conveniently between 0°C and room temperature (Rand and

Fuller, 1994). DOPE is also of considerable biological interest and affects a range of cellular functions including protein translocation (Rietveld et al., 1995).

T_{LH} of fully-hydrated DOPE (DOPE in coexistence with a bulk water phase) has been measured by a variety of methods, including differential scanning calorimetry (DSC), nuclear magnetic resonance (NMR), x-ray diffraction (XRD), Fourier-transform infra-red spectroscopy (FTIR), and fluorescence (FL) as detailed in Table 1. Despite the years of interest on this lipid and multiple experimental techniques, the resultant literature values range from -4 to 16°C (Koynova and Caffrey, 1994). This wide range of uncertainty about the true transition temperature limits the utility of DOPE thermodynamic data. Similar ambiguities plague almost all mesomorphic lipid phase transitions, with the result that the phase diagrams of most lipid–water systems are poorly known.

The wide range of published T_{LH} values is a consequence of the kinetically hindered nature of the L_{α} – H_{II} transition, with the consequence that the temperature at which the transition occurs is dependent upon the rate at which the temperature is changed. Even temperature changes of only a small fraction of a degree per day are insufficient to obtain the true equilibrium phase (Tate et al., 1992), which limits the use of almost all methods used to directly determine T_{LH} . The physical basis for the kinetic barriers between the lamellar and inverse hexagonal phases arise from the very different geometry of the water–lipid interfaces in the two phases (Fig. 1). There is no simple path for the lipid–water interfaces to transform between the phases without tearing and reorganizing, which implies that the transition involves substantial exposure of the hydrocarbon chains to water. Such topologically hindered transitions are very common

Submitted October 24, 2001, and accepted for publication December 3, 2001.

Address reprint requests to Gilman E.S. Toombes, 192 Clark Hall, Cornell University, Ithaca, NY 14853. Tel.: 607-255-8678; Fax: 607-255-8678; E-mail: getl@cornell.edu.

© 2002 by the Biophysical Society

0006-3495/02/05/2504/07 \$2.00

TABLE 1 Determinations of the L_{α} : H_{II} phase transition temperature

Year	Lipidat	Reference	Method	T_{LH} ($^{\circ}C$)
1985	6368	(Kirk and Gruner, 1985)	XRD	7.5
1988	4769	(Crowe et al., 1988)	FTIR	8
1988	4153	(Gruner, et al., 1988)	XRD	7.5
1989	7676	(Wistrom et al., 1989)	DSC (0.33 $^{\circ}C$ /min)	8
1990	9340	(Cheng, 1992)	FL(ANS)	10
1992	11831	(Fenske and Cullis, 1992)	NMR	11.5
1992	13210	(Gawrisch, et al., 1992)	NMR	-1.5-6
1993	18303	(Sanderson et al., 1993)	DSC (\pm 300 $^{\circ}C$ /hour)	-4-16
1994	17592	(Osman and Cornell, 1994)	^{31}P NMR	0.5-6.5 ($T_{avg} = 2^{\circ}C$)

From Koynova and Caffrey, (1994).

with biomembrane lipids and, more generally, are also seen with other amphiphilic systems, such as diblock copolymers. These phase transitions typically exhibit hysteresis, that is to say, the apparent phase transition temperature upon heating is higher than upon cooling. Another characteristic is that the amount of hysteresis generally increases with the degree of segregation of the amphiphile molecules, which may be readily understood in terms of the free energy cost of exposing one part of the amphiphile to the environment of the other. Thus, short lysolipids tend to exhibit less hysteresis than long-chain lysolipids, which, in turn, have less hysteresis than long-chain diacyl lipids (Tenchov, 1991).

The goal of this study is to accurately determine T_{LH} for DOPE by examining the systematic behavior of the directly measured, apparent rate-dependent transition temperature, $T_A(r)$, upon the rate of temperature change, r . This approach was inspired by analogous studies on block copolymer systems (Ryu and Lodge, 1999). The method, which has been developed here, is generally applicable to other lipid systems.

MATERIALS AND METHODS

Sample preparation

DOPE was obtained from Avanti Polar Lipids (Alabaster, AL) and used without additional purification. A clean stock solution of DOPE was

prepared by solubilization in spectrophotometry grade cyclohexane obtained from Fisher Scientific (Fair Lawn, NJ) (100 mg DOPE:1 ml cyclohexane) and stored at $-70^{\circ}C$. Lipid purity was checked before and after data collection by thin layer chromatography.

Individual samples were prepared by lyophilizing 5 mg of DOPE in a narrow ($d = 2.5$ mm) glass tube. Ten microliters of deionized water was added, and the sample homogenized by five freeze-thaw-mixing cycles. In each cycle, samples were frozen at $-70^{\circ}C$, warmed to room temperature, centrifuged for 5 min and mechanically mixed for 5 min with a 10- μ L Drummond Microdispenser (Broomall, PA). The resultant lipid gel was transferred to an acid-cleaned 1 mm glass x-ray capillary (Charles Supper, Natick, MA) and 5 μ L excess water added on top before sealing with a layer of vacuum grease backed with an epoxy plug. A small air bubble was used to separate lipid and the sealing materials. Prior to data collection, samples were cycled an additional 5 times between $-20^{\circ}C$ and $20^{\circ}C$. Each cycle lasted for approximately 10 min.

Thermal cycling protocol

Previous studies of DOPE phase behavior showed that sample history is reset by cooling well into the L_{β} phase (Shyamsunder et al., 1988). Each thermal cycle commenced with 30 min equilibration at $T_{min} = -20^{\circ}C$. X-ray diffraction data were gathered as the temperature was progressively incremented ($\Delta T = 0.1^{\circ}C$) to $T_{max} = 20^{\circ}C$. After 30 min equilibration at T_{max} , the temperature was decremented back to T_{min} . For both temperature increments and decrements, the maximum and minimum rates of temperature change were $r = 6.25 \times 10^{-2}$ and $5.9 \times 10^{-5}^{\circ}C/s$, respectively. For slow scans, the sample temperature was ramped at an intermediate scan speed of $r = 2.5 \times 10^{-4}$ for $|T - T_{LH}| > 5^{\circ}C$. Temperature stability was better than $0.05^{\circ}C$ as measured with a second resistance temperature detector (RTD) used in place of the sample.

X-ray scattering

Small angle x-ray scattering (SAXS) data were obtained using an RU-200 Cu rotating anode X-ray generator (Rigaku, The Woodlands, TX) directed through a nickel filter and single Franks mirror ($q_{min} = 0.025 \text{ \AA}^{-1}$). The flux at the sample was 2×10^7 Cu K_{α} x-rays ($\lambda = 1.54 \text{ \AA}$) per second (Tate, 1987). The sample stage temperature was measured with a platinum RTD sensor (Omega Inc., Stamford, CT) and regulated with a water-cooled Peltier device operating within the beamline vacuum. Eight-second exposures provided sufficient scattering intensity and the read-out from the home-made CCD area detector (Tate et al., 1997) also took 8 s. This set the maximum thermal scan rate at 16 s per temperature step.

Visualizing phase transitions

Because the sample consists of many small, randomly-ordered crystallites, the scattering intensity per unit area, $I(q)$, may be averaged radially as a

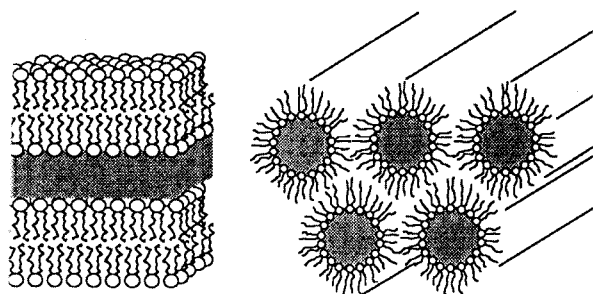


FIGURE 1 Lipid organization in the lamellar liquid (L_{α}) and (H_{II}) phases (Tate, 1987). In both phases, lipid molecules are arranged such that the polar headgroups (circles) form an interface separating the water (gray region) from the oily hydrocarbon tails.

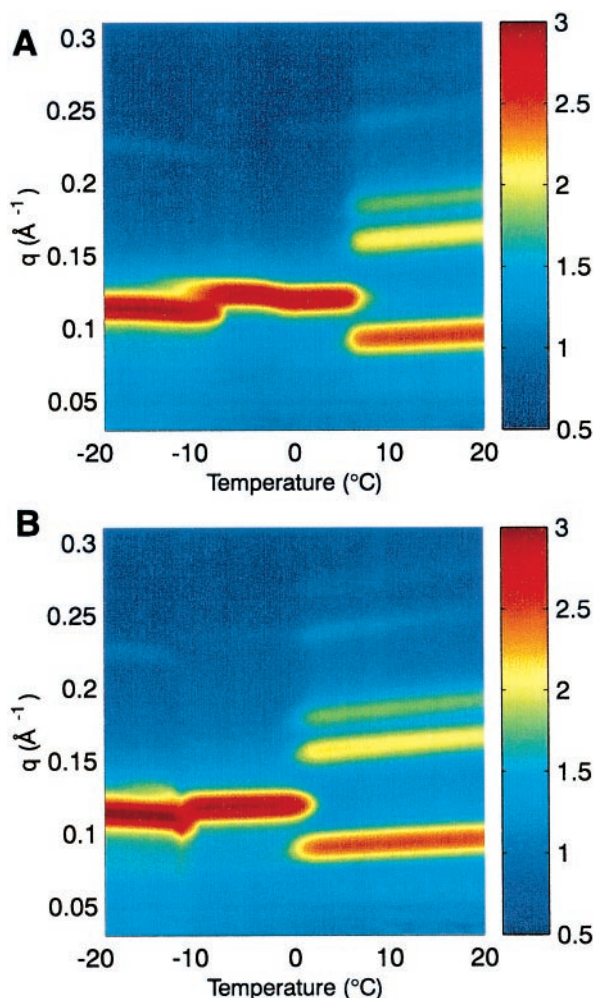


FIGURE 2 $\log(I(q))$ plotted in false color as a function of q and T for (A) heating and (B) cooling at a rate of $r = 2.86 \times 10^{-4} \text{C/s}$. A vertical slice at temperature T shows the scattering from the sample at that temperature. The phase composition of the sample may be directly determined from the scattering pattern. For the heating scan (A), the L_{β} - L_{α} transition occurs at $T \approx -9^{\circ}\text{C}$ and the L_{α} - H_{II} transition at $T \approx 6^{\circ}\text{C}$. Upon cooling (B), the H_{II} - L_{α} transition is at $T \approx 0.5^{\circ}\text{C}$ and the L_{α} - L_{β} transition occurs at $T \approx -12^{\circ}\text{C}$.

function of the scattering vector magnitude, $q = 4\pi \sin(\theta)/\lambda$, where 2θ is the total scattering angle. The H_{II} phase scatters into peaks with a q -spacing ratio of $1:\sqrt{3}:2$ while the L_{α} phase scatters into peaks with a ratio of $1:2:3$.

Sample diffraction for a thermal scan was visualized with false-color images as shown in Fig. 2. Using color to represent $I(q)$, scattering is recorded as a function of q and temperature, T . Horizontal slices show the evolution of scattering at a given q mode, whereas vertical slices of the image show sample ordering at a particular temperature. The scattering signatures of the lamellar and hexagonal phases are distinct.

Determining apparent transition temperatures

Figure 2 shows that transitions occur over a finite range of temperature. The fraction, f , of the sample in a given phase is proportional to the x-rays scattered into diffraction peaks of that phase. Figure 3 shows the integrated scattering of the H_{II} phase peaks for heating and cooling. The scattered

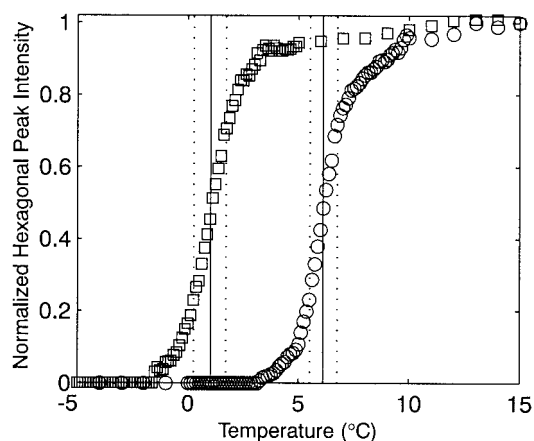


FIGURE 3 Normalized intensity of H_{II} phase peaks versus temperature for heating (\circ) and cooling (\square) at $r = 2.86 \times 10^{-4} \text{C/s}$. On heating, 50% conversion occurs at $T_{A\uparrow} = 6.11 \pm 0.64^{\circ}\text{C}$, whereas, on cooling, $T_{A\downarrow} = 1.03 \pm 0.76^{\circ}\text{C}$. The transitions are marked with solid lines and the 25–75% range is marked with dotted lines.

intensity for a given phase component is normalized relative to the signal when 100% of the sample is in that phase. The finite temperature range, ΔT_A , for conversion demands a functional definition of the apparent transition temperature, T_A . For the purposes of this analysis, T_A is defined as the temperature when 50% of the sample has entered the final phase. ΔT_A is defined using the 75% occupancy of the initial and final phases. For heating, at $T = T_A - \Delta T_A$, 75% of the sample is in the initial phase, but, when $T = T_A + \Delta T_A$, 75% of the sample is in the final phase. These points are all marked on Fig. 3. For each thermal cycle, an apparent transition temperature for heating, $T_{A\uparrow}$ and for cooling, $T_{A\downarrow}$ is assigned along with transition widths $\Delta T_{A\uparrow}$ and $\Delta T_{A\downarrow}$.

RESULTS

Figure 4 shows T_A as a function of r . For a given scan rate,

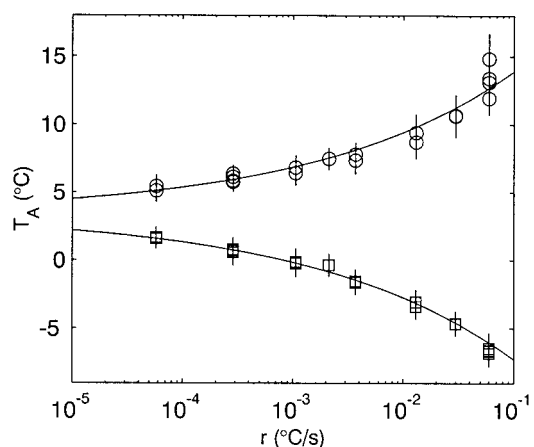


FIGURE 4 Apparent transition temperature, T_A , versus rate of heating/cooling, r . Heating scans are marked as (\circ) and cooling scans are marked as (\square). Error bars represent the 25% and 75% mark of the transition. The fitted line is of the form, $T_A = T_{LH} \pm \alpha r^{\beta}$ where $T_{LH} = 3.33 \pm 0.16^{\circ}\text{C}$, $\beta = 0.2401 \pm 0.0060$ and $\alpha = 18.41 \pm 0.71^{\circ}\text{C}^{1-\beta}\text{s}^{\beta}$.

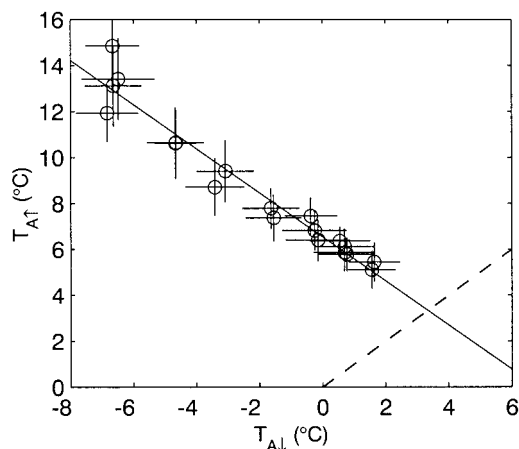


FIGURE 5 Apparent transition temperature on heating, $T_{A\uparrow}$, versus apparent transition temperature on cooling, $T_{A\downarrow}$. A linear extrapolation of $T_{A\uparrow}$ (solid line) to intersect the line $T_{A\uparrow} = T_{A\downarrow}$ (dashed line) gives a transition temperature of $T_{LH} = 3.33 \pm 0.16^\circ\text{C}$. The slope of the extrapolation is -0.961 ± 0.051 .

the apparent transition temperature on heating, $T_{A\uparrow}$, and apparent transition temperature on cooling, $T_{A\downarrow}$, were found to be independent of sample used or number of thermal cycles. Transition hysteresis is pronounced but the weak dependence on scanning rate rules out Arrhenius-type kinetics. The broad range of applied temperature rates and the symmetry between heating and cooling hysteresis permits a determination of T_{LH} by extrapolation.

Determination of T_{LH}

Determining the limits, $\lim_{r \rightarrow 0} T_{A\uparrow}(r) = T_{LH}$ or $\lim_{r \rightarrow 0} T_{A\downarrow}(r) = T_{LH}$ directly requires a specific model for hysteresis. Much can be determined, however, without resorting to particular models. At the limit $r = 0$, $T_{A\uparrow}(r) = T_{A\downarrow}(r)$. $T_{A\downarrow}$ and $T_{A\uparrow}$ are likely to satisfy the relation,

$$0 < r_1 < r_2 \Rightarrow T_{A\downarrow}(r_2) < T_{A\downarrow}(r_1) < T_{LH} < T_{A\uparrow}(r_1) < T_{A\uparrow}(r_2), \quad (1)$$

making $T_{A\uparrow}$ a single-valued function of $T_{A\downarrow}$. The intersection of this derived function, $T_{A\uparrow}(T_{A\downarrow})$, with the line $T_{A\uparrow} = T_{A\downarrow}$ is the transition temperature, T_{LH} .

Figure 5 is a plot of $T_{A\uparrow}$ versus $T_{A\downarrow}$ for each thermal cycle. Cooling data range from $-6.7^\circ\text{C} < T_{A\downarrow} < 1.6^\circ\text{C}$ whereas transitions on heating occurred between $5.3^\circ\text{C} < T_{A\uparrow} < 13.4^\circ\text{C}$. To determine T_{LH} , the curve $T_{A\uparrow}(T_{A\downarrow})$ must be extrapolated 20% beyond the measured range. The function is well approximated by a straight line and a least-squares fit is shown on Fig. 5. Extrapolating the fit yields $T_{LH} = 3.33 \pm 0.16^\circ\text{C}$. Direct measurements only limit the transition temperature to $1.6^\circ\text{C} < T_{LH} < 5.3^\circ\text{C}$, and even at low scan speeds T_A exhibited a width of $\Delta T_A = 0.8^\circ\text{C}$.

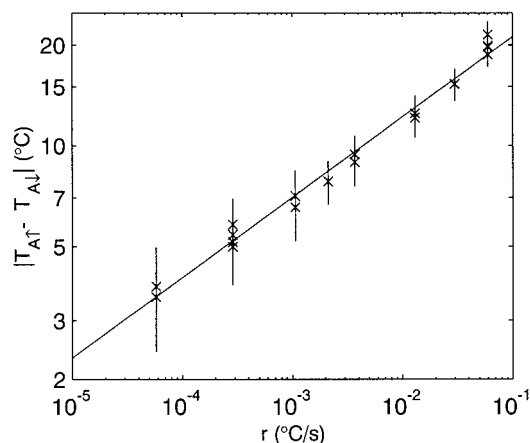


FIGURE 6 Loop hysteresis, $|T_{A\uparrow} - T_{A\downarrow}|$, versus rate of heating or cooling, r . The log-log plot fit has a slope of 0.2401 ± 0.0060 and an intercept of $36.8 \pm 1.4^\circ\text{C}$. Slowing thermal scan speed by $16\times$ reduces transition hysteresis by only $2\times$.

Cycle hysteresis

There are many mechanisms that cause hysteresis in first-order phase transitions, each producing a functional dependence on scanning rate. Figure 6 shows loop hysteresis $|T_{A\uparrow}(r) - T_{A\downarrow}(r)|$ as a function of r . Reduction of the scan rate by 1.06×10^3 only diminished $|T_{A\uparrow} - T_{A\downarrow}|$ by a factor of 4.5 ± 1.0 . Hysteresis over the entire range is well fit by the equation,

$$|T_{A\uparrow} - T_{A\downarrow}| = 2\alpha r^\beta, \quad (2)$$

where $\alpha = 18.4 \pm 0.7^\circ\text{C}^{1-\beta}\text{s}^\beta$ and $\beta = 0.2401 \pm 0.0060$. The root mean square variation for a given cycle from the power-law fit is only 6.4%.

Symmetry of heating and cooling

The $L_{\alpha} \rightarrow H_{II}$ and $H_{II} \rightarrow L_{\alpha}$ kinetic pathways may be compared by studying $T_{A\uparrow}(r)$ and $T_{A\downarrow}(r)$ as shown in Fig. 4. Remarkably, both transitions fit the functional form,

$$T_A = T_{LH} \pm \alpha r^\beta, \quad (3)$$

where $T_{LH} = 3.33 \pm 0.16^\circ\text{C}$, $\beta = 0.2401 \pm 0.0060$, and $\alpha = 18.41 \pm 0.71^\circ\text{C}^{1-\beta}\text{s}^\beta$. Neither $L_{\alpha} \rightarrow H_{II}$ nor $H_{II} \rightarrow L_{\alpha}$ kinetics show significant systematic deviation from this power-law relationship.

Transition width

T_A has a clear dependence on scan rate r . The transition width, ΔT_A , is not so predictable, as Fig. 7 illustrates. On average, ΔT_A should be a monotonic increasing function of r . No such broad trend is evident, although, for heating rates above $r = 10^{-2}\text{C/s}$, the transition width does seem to grow.

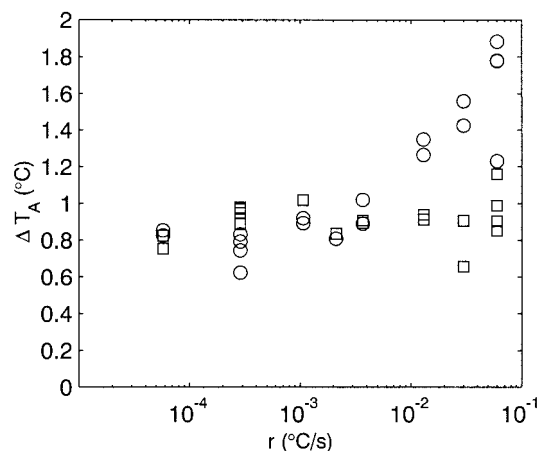


FIGURE 7 Width of transition, ΔT_A , versus rate, r , for heating (○) and cooling (□). No universal trend is prevalent, suggesting that sample inhomogeneity may dominate transition width.

DISCUSSION

Comparison to previous values

By extrapolation, $T_{LH} = 3.33 \pm 0.16^\circ\text{C}$ for fully hydrated DOPE. The finite transition width ΔT_A observed for all thermal ramping speeds is the dominant source of uncertainty in determining T_{LH} . Results summarized in Table 1 place a lower bound of 0.5°C , and data from Tate et al. (1992) (shown in Table 2) suggest an upper bound of 4°C . The current determination is consistent with other reports and provides confidence in a more precise value of T_{LH} .

Determining hysteretic transitions

Metastable states and hysteretic transitions are prevalent in biology, but determining the location of hysteretic transitions is experimentally challenging (Tenchov, 1991). For a fixed thermal scan rate, the phase transition occurs rapidly at a temperature, T_A , that is reproduced on every scan. Furthermore, reducing scan rate only has a small effect on T_A . This can give the impression that the system is close to

equilibrium when in truth $|T_A - T_{LH}|$ is large, as is easily demonstrated for reversible hysteretic transitions.

The DOPE L_α - H_{II} transition is remarkable for the symmetry between forward and reverse hysteresis. In the general case, the empirical form of $T_A(r)$ suggests r must be varied by well over an order of magnitude for even a rough estimate of hysteresis. This places x-ray scattering, NMR, and other “absolute” measures of phase at an advantage over DSC and other differential techniques that restrict the range of scan speeds. Transitions of this type must be tested over a very wide set of equilibration times.

DOPE transition kinetics

Most studies of L_α - H_{II} phase kinetics for DOPE have utilized large temperature and pressure jumps to aid the search for transition intermediates (Erbes et al., 2000). Conversion rates depend heavily on jump size for large jumps. Ramping data only partially describes phase conversion kinetics as it convolutes the effects of the individual steps involved. A common hypothesis is that phase conversion pathway is independent of rate so that,

$$\frac{df}{dt} = h(f)g(T - T_{LH}), \quad (4)$$

where f is the fraction in the new phase, $h(f)$ is the conversion mechanism function, and $g(T - T_{LH})$ is the rate of conversion (Kennedy and Clark, 1996). The combination of this model with the measured form of $T_A(r)$ (Eq. 2) requires that,

$$\text{Rate of Conversion} \propto |T - T_{LH}|^{1/\beta-1}, \quad (5)$$

where $\beta \approx 0.25$. Regardless of the ansatz used in Eq. 4, at slow rates, phase conversion kinetics demonstrably follow a power-law term. Tate et al.’s (1992) study of conversion kinetics under small temperature jumps (Table 2) supports this conclusion. Many rate-limiting mechanisms could produce a power-law relationship, but the data cannot be reconciled with the exponential behavior of single activation barrier models (Kennedy and Clark, 1996).

Determination of rate-limiting steps

Phase conversion in DOPE may be limited by nucleation, inaccessible intermediate states for domain growth, or barriers to bulk water transport. This study shows that, whatever the detailed mechanism, the same rate-limiting process applies over three orders of magnitude of conversion rate! The precise identity of the rate-limiting mechanism should be revealed by study of conversion kinetics under altered conditions.

Tristram-Nagle et al. (1994) determined nucleation to be important in sub-gel formation of DPPC with a two-temperature-jump protocol. An identical procedure could be

TABLE 2 Transition times as determined for a DOPE sample undergoing an abrupt temperature step

Temperature (°C)	25% Conversion (s)	50% (s)	75% (s)
-5.0	2.58	6.24	12.5
-2.0	23.0	55.5	110.9
0.0	264	636	1273
4.0	15720	60640	303360
6.0	156	384	813
8.0	28	67.9	136
20.0	5.8	13.9	27.7

From Tate et al. (1992).

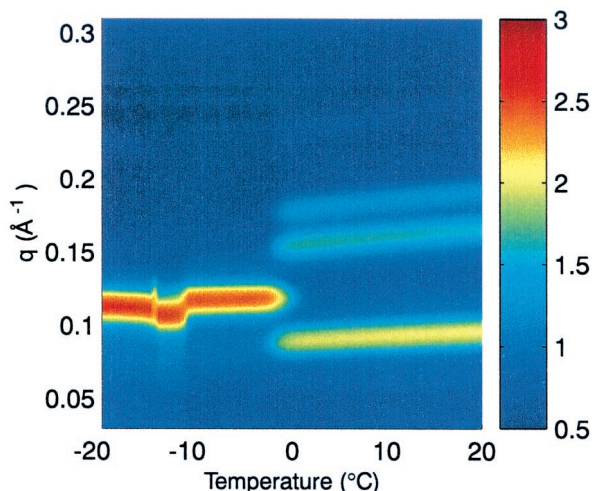


FIGURE 8 Scattering intensity for cooling scan at $r = 3.70 \times 10^{-3} \text{ } ^\circ\text{C s}^{-1}$. There are two abrupt changes in D-spacing in the vicinity of the L_{α} - L_{β} transition ($T \approx -12^\circ\text{C}$).

used for DOPE. Limitations imposed by water transport should have two characteristic signatures. Above 22°C , the H_{II} phase is energetically preferred over the L_{α} phase at all hydrations (Gawrisch et al., 1992) so more rapid heating should show a dramatic increase in conversion speed above 22°C if water transport is rate limiting. An alternative approach would be to study samples with reduced water concentrations. At a concentration of 11 ± 1 water molecules per lipid (Gawrisch et al., 1992) there is no change in hydration between L_{α} and H_{II} phases that would limit conversion speed. Finally, the role of intermediates can be tested by adding small quantities of lyso-lipids and other impurities (Gruner et al., 1988). Regrettably, sample preparation can markedly alter phase conversion kinetics (Epan and Lemay, 1993), so such studies will be quite challenging.

Ice formation

Sanderson et al., (1993) demonstrated the importance of ice formation in lipid:water samples. This experiment has shown that the bulk freezing point of water is not significant for the L_{α} - H_{II} phase transition under slow-to-moderate conversion. Ice formation should cause an asymmetry in hysteresis between heating and cooling and cause an abrupt change in L_{α} repeat spacing. Neither effect was observed. Bulk ice formation might explain the two abrupt changes in lamellar repeat spacing in the L_{β} - L_{α} transition as shown in Fig. 8. However, Epan and Epan (1988) report a two-step liquid-gel transition for DEPE at slow scan rates ($T_{\text{trans}} > 35^\circ\text{C}$), so ice formation is not an essential explanation in our experiment.

CONCLUSION

Experiments upon lipid liquid crystals are greatly complicated by hysteresis and metastability. Using linear temperature ramps, this study has shown that the L_{α} - H_{II} phase transition in a bulk sample of DOPE is highly reproducible. When the sample is heated or cooled at a fixed rate, r , the apparent phase conversion temperature, $T_A(r)$, is well defined, and conversion occurs over a relatively small temperature range, $\Delta T_A(r)$. By measuring $T_A(r)$ over three orders of magnitude of r , an accurate extrapolation of the L_{α} - H_{II} transition temperature was possible and was found to be $T_{LH} = 3.33 \pm 0.16^\circ\text{C}$.

The functional form of $T_A(r)$ proved to be particularly interesting. Hysteresis was identical for heating and cooling following the equation,

$$T_A(r) = T_{LH} \pm \alpha |r|^\beta \quad \beta \approx 0.25. \quad (6)$$

This power-law dependence is unexpected and conflicts with the exponential form of single-activation barrier kinetics. The study provides no direct insight into the rate-limiting step in topological transitions, although the precise characterization of phase conversion kinetics for fully hydrated DOPE is an excellent basis for further investigations. Although hysteresis can be very significant in lyotropic phase transitions and may cause substantial errors when determining thermodynamic parameters, this study shows that a careful analysis of rate-dependent trends can accurately eliminate almost all of the rate dependence from the transition-temperature determination.

REFERENCES

- Brown, M. F. 1997. Influence of Non-lamellar forming lipids on rhodopsin. *Curr. Topics Membr.* 44:285–356.
- Cheng, K. 1990. Headgroup hydration and motional order of lipids in lamellar liquid crystalline and inverted hexagonal phases of unsaturated phosphatidylethanolamine—a time-resolved study. *Chem. Phys. Lipids.* 53:191–202.
- Crowe, J., F. Hoekstra, and L. Crowe. 1988. Gel to liquid crystalline phase transitions are responsible for leakage from dry pollen during rehydration. *Biophys. J.* 53:129a.
- Epan, R. M., and R. F. Epan. 1988. Kinetic effects in the differential scanning calorimetry cooling scans of phosphatidylethanolamines. *Chem. Phys. Lipids.* 49:101–104.
- Epan, R. M., and C. T. Lemay. 1993. Lipid concentration affects the kinetic stability of dielaidoylphosphatidylethanolamine bilayers. *Chem. Phys. Lipids.* 66:181–187.
- Erbes, J., A. Gabke, G. Rapp, and R. Winter. 2000. Kinetics of phase transformations between lyotropic lipid mesophases of different topology: a time-resolved synchrotron x-ray diffraction study using the pressure-jump relaxation technique. *Phys. Chem. Chem. Phys.* 2:151–161.
- Fenske, D., and P. Cullis. 1992. Chemical exchange between lamellar and non-lamellar lipid phase—a one and two-dimensional phosphorus-31 NMR study. *Biochim. Biophys. Acta.* 1108:201–209.
- Gawrisch, K., V. A. Parsegian, D. A. Hajduk, M. W. Tate, S. M. Gruner, N. L. Fuller, and R. P. Rand. 1992. Energetics of a hexagonal-lamellar-hexagonal-phase transition sequence in dioleoylphosphatidylethanolamine membranes. *Biochemistry.* 31:2856–2864.

- Gruner, S., M. Tate, G. Kirk, P. So, D. Turner, D. Keane, C. Tilcock, and P. Cullis. 1988. X-ray diffraction study of the polymorphic behavior of *N*-methylated dioleoylphosphatidylethanolamine. *Biochemistry*. 27: 2853–2866.
- Hazel, J. R., and E. E. Williams. 1990. The role of alterations in membrane lipid composition in enabling physiological adaptation of organisms to their physical environment. *Prog. Lipid Res.* 29:167–227.
- Kennedy, J. A., and S. M. Clark. 1996. A general method for the analysis of non-isothermal kinetic data. *Materials Sci. Forum.* 228–231: 423–428.
- Kirk, G., and S. Gruner. 1985. Lyotropic effects of alkanes and headgroup composition on the L_{α} - H_{II} lipid liquid crystal phase transition: hydrocarbon packing versus intrinsic curvature. *J. Physiq.* 46:761–769.
- Koynova, R., and M. Caffrey. 1994. Phases and phase transitions of the hydrated phosphatidylethanolamines. *Chem. Phys. Lipids.* 69:1–34.
- Kuzmin, P. I., J. Zimmerberg, Y. A. Chizmadzhev, and F. S. Cohen. 2001. A quantitative model for membrane fusion based on low energy intermediates. *Proc. Natl. Acad. Sci. U.S.A.* 98:7235–7240.
- Nagle, J. F., and H. L. Scott. 1978. Biomembrane phase transitions. *Physics Today*. (2):p39.
- Osman, P., and B. Cornell. 1994. The effect of pulsed electric fields on the phosphorus-31 spectra of lipid bilayers. *Biochim. Biophys. Acta.* 1195: 197–204.
- Rand, R. P., and N. L. Fuller. 1994. Structural dimensions and their changes in a reentrant hexagonal-lamellar transition of phospholipids. *Biophys. J.* 68:2127–2138.
- Rietveld, A. G., M. C. Koorengel, and B. de Kruijff. 1995. Non-bilayer lipids are required for efficient protein transport across the plasma membrane of *Escherichia coli*. *EMBO J.* 14:5506–5513.
- Ryu, C. Y., and T. P. Lodge. 1999. Thermodynamics, stability and anisotropic fluctuations in the cylinder-to-sphere transition of a block copolymer. *Macromolecules.* 32:7190–7201.
- Sanderson, P. W., W. P. Williams, B. A. Cunningham, D. H. Wolfe, and L. J. Lis. 1993. The effect of ice on membrane lipid phase behavior. *Biochim. Biophys. Acta.* 1148:278–284.
- Shyamsunder, E., S. M. Gruner, M. W. Tate, D. C. Turner, P. T. C. So, and C. P. S. Tilcock. 1988. Observation of inverted cubic phase in hydrated dioleoylphosphatidylethanolamine membranes. *Biochemistry.* 27: 2332–2336.
- Tardieu, A., V. Luzzati, and F. C. Reman. 1973. Structure and polymorphism of the hydrocarbon chains of lipids: a study of lecithin–water phases. *J. Mol. Biol.* 75:711–733.
- Tate, M. W. 1987. Equilibrium and kinetic states of the L_{α} - H_{II} phase transition. Ph.D. Thesis, Princeton University, Princeton, NJ.
- Tate, M. W., S. M. Gruner, and E. F. Eikenberry. 1997. Coupling format variations in x-ray detectors based on charged coupled devices. *Rev. Sci. Instrum.* 68:47–54.
- Tate, M. W., E. Shyamsunder, S. M. Gruner, and K. L. D'Amico. 1992. Kinetics of the lamellar-inverse hexagonal phase transition determined by time-resolved x-ray diffraction. *Biochemistry.* 31:1081–1092.
- Tenchov, B. 1991. On the reversibility of the phase transitions in lipid–water systems. *Chem. Phys. Lipids.* 57:165–177.
- Tristram-Nagle, S., R. M. Suter, W.-J. Sun, and J. F. Nagle. 1994. Kinetics of subgel formation in DPPC: x-ray diffraction proves nucleation-growth hypothesis. *Biochim. Biophys. Acta.* 1191:14–20.
- Wistrom, C., R. Rand, L. Crowe, B. Spargo, and J. Crowe. 1989. Direct transition of dioleoylphosphatidylethanolamine from lamellar gel to inverted hexagonal phase caused by trehalose. *Biochim. Biophys. Acta.* 984:238–242.